AIP Journal of Applied Physics

Generalizing Murray's law: An optimization principle for fluidic networks of arbitrary shape and scale

David Stephenson, Alexander Patronis, David M. Holland, and Duncan A. Lockerby

Citation: Journal of Applied Physics **118**, 174302 (2015); doi: 10.1063/1.4935288
View online: http://dx.doi.org/10.1063/1.4935288
View Table of Contents: http://scitation.aip.org/content/aip/journal/jap/118/17?ver=pdfcov
Published by the AIP Publishing

JOURNAL OF APPLIED PHYSICS **118**, 174302 (2015)

Generalizing Murray's law: An optimization principle for fluidic networks of arbitrary shape and scale

David Stephenson,[a] Alexander Patronis,[b] David M. Holland,[c] and Duncan A. Lockerby[d]
School of Engineering, University of Warwick, Coventry, CV4 7AL, United Kingdom

(Received 17 August 2015; accepted 26 October 2015; published online 6 November 2015)

Murray's law states that the volumetric flow rate is proportional to the cube of the radius in a cylindrical channel optimized to require the minimum work to drive and maintain the fluid. However, application of this principle to the biomimetic design of micro/nano fabricated networks requires optimization of channels with arbitrary cross-sectional shape (not just circular) and smaller than is valid for Murray's original assumptions. We present a generalized law for symmetric branching that (a) is valid for any cross-sectional shape, providing that the shape is constant through the network; (b) is valid for slip flow and plug flow occurring at very small scales; and (c) is valid for networks with a constant depth, which is often a requirement for lab-on-a-chip fabrication procedures. By considering limits of the generalized law, we show that the optimum daughter-parent area ratio Γ, for symmetric branching into N daughter channels of any constant cross-sectional shape, is $\Gamma = N^{-2/3}$ for large-scale channels, and $\Gamma = N^{-4/5}$ for channels with a characteristic length scale much smaller than the slip length. Our analytical results are verified by comparison with a numerical optimization of a two-level network model based on flow rate data obtained from a variety of sources, including Navier-Stokes slip calculations, kinetic theory data, and stochastic particle simulations.
 [http://dx.doi.org/10.1063/1.4935288]

I. INTRODUCTION

In 1926, Murray[1] posited that there were two competing factors contributing to the energy cost of blood flow through the arterial system: (1) the energy required to drive the flow, which increases as the vessel radius decreases; and (2) the energy required to metabolically maintain the fluid, which increases with increasing vessel radius. Thus, to minimize the total power requirement, the vessel could be neither too large nor too small. Using the Hagen-Poiseuille law to describe the flow through a cylindrical vessel (i.e., assuming the flow is laminar, Newtonian, steady, and fully developed), the power W_f required for the flow to overcome the viscous drag is

$$W_f = f\Delta P = \frac{8\mu L f^2}{\pi r^4}, \tag{1}$$

where ΔP is the pressure drop over the vessel, μ is the dynamic viscosity of the fluid, L is the vessel length, f is the volumetric flow rate, and r is the vessel radius. This is offset by the maintenance "cost of blood" W_m which increases linearly with the blood volume:

$$W_m = mL\pi r^2, \tag{2}$$

where m is an all-encompassing metabolic coefficient that includes the chemical cost of keeping the blood constituents fresh and functional, and the general cost owing to the weight of the blood and the vessel. The total power requirement $W_t = W_f + W_m$ is thus

$$W_t = \frac{af^2}{r^4} + br^2, \tag{3}$$

where $a = 8\mu L/\pi$ and $b = m\pi L$. For a constant volumetric flow rate, and given values of a and b, the total power will be a function of a single variable—the vessel radius r—and the minimum power is found by differentiating with respect to r and equating to zero:

$$\frac{dW_t}{dr} = \frac{-4af^2}{r^5} + 2br = 0. \tag{4}$$

Rearranging Eq. (4) gives

$$f = \mathcal{K} r^3, \tag{5}$$

where $\mathcal{K} = \sqrt{b/2a}$. Thus for any vessel considered independently, Eq. (5) describes the optimal relation between volumetric flow rate and vessel radius, such that the power requirement is minimized. If the fluid viscosity and metabolic coefficient are constant throughout a network, then $\mathcal{K}$ is constant. It was surmised that in this instance, Eq. (5) should hold for all vessels in a network operating at maximum efficiency, which tacitly assumes that the local losses through the junction (due to bends and channel contractions) are negligible compared to the pressure losses over the channel lengths; this limits the applicability of Murray's law to networks of high-aspect-ratio channels. By applying the conservation of mass at a branching point, we retrieve the ubiquitous principle known as Murray's law:

[a]david.stephenson@warwick.ac.uk
[b]a.patronis@warwick.ac.uk
[c]d.m.holland@warwick.ac.uk
[d]duncan.lockerby@warwick.ac.uk

$$r_p^3 = \sum_{i=1}^{N} r_{d_i}^3, \tag{6}$$

where the subscripts p and d_i denote the parent and the ith daughter (of N), respectively. In the common case of symmetrical branching, Eq. (6) reduces to

$$r_p^3 = N r_d^3. \tag{7}$$

Murray's law has been shown to be a good approximation for a diverse range of biological networks whose primary function is fluidic transport, for example, in the cardiovascular systems of multiple animals;[2–9] in the bronchial trees of lungs;[10–12] and in the leaf veins of plants.[13–15] Murray's law can also be applied to inorganic systems[5] and has been adapted for networks with rectangular, trapezoidal,[16] and elliptical cross sections.[17] The applicability of Murray's law to moderately rarefied gas flows has also been investigated[18] and a departure from Eq. (7) has been noted. These developments indicate that some version of Murray's law could be applied as a biomimetic design principle for microfluidic and nanofluidic networks, such as lab-on-a-chip devices for microreactors[19] or tissue engineering,[20] or micro/nanoscale heat exchangers for high performance fuel cells[21] or the cooling of electronic devices.[22,23]

Since the original derivation of Murray's law, it has been noted that the application of other optimization principles (not just that of minimum work) result in Eq. (7): minimizing the total mass of the network,[24] minimizing volume for a constant pressure drop and flow rate,[25] keeping the shear stress constant in all channels,[26] or minimizing flow resistance for a constant volume.[5,27]

As noted in Ref. 16, in some circumstances, it is desirable or necessary for the cross-sectional shape to vary between the parent and daughter channels of a branching network. In many lab-on-a-chip fabrication procedures (e.g., photolithograpy, wet or dry etching, or surface micromachining), the depth remains constant throughout the device, and thus the shape (i.e., aspect ratio) of the cross section must vary. A multi-depth approach to fabrication does exist,[28] but it is relatively complex.

Despite many developments to Murray's law, there are three major barriers that prevent it from being relevant to the design of many artificial fluidic networks: (1) it is not demonstrably applicable to cross sections of any arbitrary shape; (2) it is not applicable at the micro/nanoscale, where a fluid can no longer be accurately described as a continuous material;[29] and (3) it is not applicable to networks which maintain a constant depth through branching, wherein the cross-sectional shape changes between the parent and daughter channels.

II. ANALYTICAL SOLUTIONS

Although Murray's original optimization concerns the minimization of work, the principle can be generalized as a maximization of flow conductance per unit volume for a variety of constraint combinations. For a two-level network (consisting of a single parent channel branching into multiple daughter channels), this can be expressed as

$$\arg \max_{\Gamma \in [0,\infty]} \left[\frac{Q}{\Delta P V} \right] \text{ subject to fixed } \begin{cases} Q, \Delta P \\ V, \Delta P \\ V, Q, \end{cases} \tag{8}$$

where Q is the mass flow rate through the parent channel, ΔP is the total pressure drop (from inlet of the parent to the outlet of the daughters), V is the network volume, and

$$\Gamma = \frac{A_d}{A_p} \tag{9}$$

is the daughter-parent cross-sectional area ratio. Note, the three constraint options (pressure-drop minimization, volume minimization, and flow-rate maximization) all lead to the same optimal daughter-parent area ratio. For our optimization, we assume that the channel lengths L are large compared to the size of the parent-daughters junction so that (1) the localized pressure losses through the junction are negligible compared to the pressure drops over individual channels (as in Murray's law) and (2) the volume of the network can be considered to be the sum of the channel volumes:

$$V = A_p L_p + N A_d L_d. \tag{10}$$

This means that the channel lengths are treated as being independent of the branching angle.[30] The channel lengths are also treated as being independent of the optimal daughter-parent area ratio (as found in Murray's optimization[1]), i.e., $dL/d\Gamma = 0$. This will be verified later. Inserting Eq. (10) into the fitness function of Eq. (8), differentiating with respect to Γ, and equating to zero, gives

$$\frac{d}{d\Gamma}\left(\frac{\Delta P V}{Q}\right) = L_p \frac{dA_p}{d\Gamma} + N L_d \frac{dA_d}{d\Gamma} = 0, \tag{11}$$

noting that, for all constraint combinations, $d(\Delta P)/d\Gamma = 0$ and $dQ/d\Gamma = 0$. The pressure drop over the parent and daughter channels can be expressed in terms of the mass flow rate:

$$\Delta P_p = Q L_p k_p, \tag{12}$$

$$\Delta P_d = \frac{Q L_d k_d}{N}, \tag{13}$$

where L is the channel length and k is flow resistance per unit length, e.g., $k_p = \Delta P_p/(Q L_p)$. The pressure drop over the entire network $\Delta P = \Delta P_p + \Delta P_d$ is then

$$\Delta P = Q\left(L_p k_p + \frac{L_d k_d}{N}\right). \tag{14}$$

As $d(\Delta P)/d\Gamma = 0$ and $dQ/d\Gamma = 0$, differentiating Eq. (14) with respect to Γ gives

$$L_p \frac{dk_p}{d\Gamma} + \frac{L_d}{N}\frac{dk_d}{d\Gamma} = 0. \tag{15}$$

Substituting Eq. (15) into Eq. (11), via the chain rule, gives the generalized optimal area relation for symmetric branching:

$$\left.\frac{\mathrm{d}A}{\mathrm{d}k}\right|_p = N^2 \left.\frac{\mathrm{d}A}{\mathrm{d}k}\right|_d . \tag{16}$$

For brevity, this will be referred to as the *generalized law* to distinguish it from Murray's law. This expression is not a function of L which suggests that the optimal daughter-parent area ratio is independent of the channel lengths (and thus branching angle). Note this generalized law is valid for any Reynolds number (e.g., for turbulent flow) and for any fluid (e.g., non-Newtonian)[31] as long as local losses in the junction remain negligible. In this paper, we restrict our attention to laminar and Newtonian flows, and we now consider some important cases where A can be expressed easily as an analytical function of k.

A. The continuum-flow limit

We begin with the steady incompressible Navier-Stokes momentum equation for laminar flow through a long channel with an arbitrary cross-sectional shape, i.e.,

$$\frac{\Delta P}{L} = -\mu \nabla^2 u \,, \tag{17}$$

where u is the streamwise channel velocity. We can non-dimensionalize this using $\Delta P/L$, μ and cross-sectional area A, such that

$$1 = -\tilde{\nabla}^2 \tilde{u}, \tag{18}$$

where

$$u = \tilde{u} A \left(\frac{\Delta P}{L}\right) \frac{1}{\mu}; \quad \nabla^2 = \frac{\tilde{\nabla}^2}{A}, \tag{19}$$

and tilde denotes a dimensionless quantity or operator. We also define y, z as the axes of the cross-sectional plane, and

$$y = \tilde{y}\sqrt{A}; \quad z = \tilde{z}\sqrt{A}. \tag{20}$$

Provided the boundary conditions are fixed (which is the case for the continuum-flow limit, where the no-slip boundary condition applies), the solution of Eq. (18), $\tilde{u}(\tilde{y}, \tilde{z})$, is independent of A, ΔP, L, and μ, and is thus a property of the cross-sectional shape alone. Similarly, so is

$$S = \int_A \int \tilde{u}(\tilde{y}, \tilde{z}) \, \mathrm{d}\tilde{y} \, \mathrm{d}\tilde{z} \,. \tag{21}$$

An expression for the mass flow rate is obtained by integrating the fluid momentum over the cross-sectional area

$$Q = \rho \int_A \int u \, \mathrm{d}y \, \mathrm{d}z, \tag{22}$$

where ρ is the mass density. Substitution of Eqs. (19)–(21) into (22) gives the mass flow rate for an arbitrary cross-sectional shape

$$Q = \rho A^2 \left(\frac{\Delta P}{L}\right) \frac{S}{\mu}, \tag{23}$$

and the flow resistance per unit length

$$k = \frac{\mu}{\rho S A^2} \,. \tag{24}$$

It is assumed that the pressure drop over the network is small such that the viscosity and density are constants. For cylindrical channels, $S = 1/(8\pi)$ and Eq. (23) becomes the Hagen-Poiseuille flow rate.

1. Constant-shape networks

If the cross-sectional shape is constant throughout the network (i.e., $S = \text{const}$), substituting Eq. (24) into the generalized law (Eq. (16)) gives

$$\Gamma = N^{-2/3} \,. \tag{25}$$

Equation (25) relates the area of the parent channel to the area of the daughter channel in an optimized symmetric network. Other studies have found that Murray's law holds for some specific cross-sectional shapes (i.e., rectangles and trapezoids,[16] and ellipses[17]), but this demonstrates that Murray's law for symmetric branching is in fact applicable to any cross-sectional shape, provided the shape is constant through the network. Note this means that if the cross-sectional areas are expressed in terms of a hydraulic radius, Murray's law can be expressed in its original form (i.e., Eq. (7)) for any shape—however, this is only applicable for symmetric branching at the continuum-flow limit.

2. Constant-depth networks

For a constant-depth network, the optimal branching behavior depends on the change in shape between the parent and daughter channels, which is a function of the aspect ratio $\alpha = A/h^2$ for rectangular channels. This leads to two aspect-ratio limits for Γ (at the continuum-flow limit), as illustrated in Fig. 1. An accurate approximation of the channel shape property S for a rectangle[32] is

$$S \approx \frac{h^{2b}}{4A^b}\left[\frac{1}{3} - \frac{64h^{2b}}{\pi^5 A^b} \tanh\left(\frac{\pi A^b}{2h^{2b}}\right)\right]$$
$$\text{where } b = \begin{cases} 1 & \text{for } \alpha \geq 1 \\ -1 & \text{for } \alpha < 1, \end{cases} \tag{26}$$

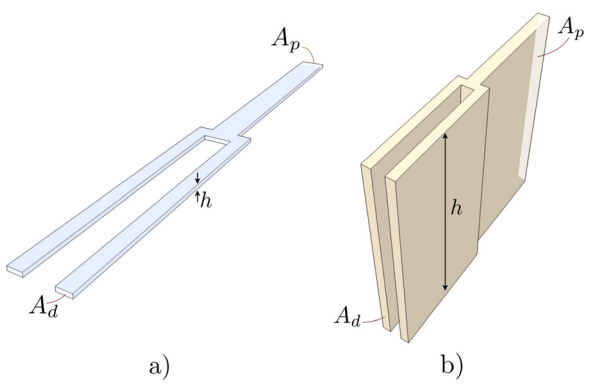

FIG. 1. Schematic showing the symmetric bifurcation of constant-depth rectangular channels of (a) high aspect ratio ($\alpha \gg 1$) and (b) low aspect ratio ($\alpha \ll 1$).

where h is the constant network depth. Equation (26) only includes the first term of an infinite series, but as the denominators of higher terms increase exponentially, the expression is sufficient. It is clear from Eq. (26) that at the aspect ratio limits, the shape property reduces to

$$S = \frac{h^2}{12A}, \quad \text{for } \alpha \gg 1; \tag{27}$$

$$S = \frac{A}{12h^2}, \quad \text{for } \alpha \ll 1. \tag{28}$$

As S is no longer a constant, the generalized law must consider the change in shape between parent and daughter channels

$$\frac{dS}{dA} = \frac{-bh^{2b}}{4A^{b+1}}\left[\frac{1}{3} - \frac{128h^{2b}}{\pi^5 A^b}\tanh\left(\frac{\pi A^b}{2h^{2b}}\right) + \frac{32}{\pi^4}\operatorname{sech}^2\left(\frac{\pi A^b}{2h^{2b}}\right)\right]. \tag{29}$$

At the aspect ratio limits, Eq. (29) reduces to

$$\frac{dS}{dA} = -\frac{h^2}{12A^2}, \text{ for } \alpha \gg 1; \tag{30}$$

$$\frac{dS}{dA} = \frac{1}{12h^2}, \text{ for } \alpha \ll 1. \tag{31}$$

Equations (30) and (31) can also be derived directly from Eqs. (27) and (28), respectively. Substituting Eqs. (24), (27), and (30) into the generalized law (Eq. (16)), via the chain rule, gives the high-aspect-ratio continuum-flow limit:

$$\Gamma = N^{-1}. \tag{32}$$

Incidentally, this limit is equal to da Vinci's rule of tree branching.[33] Similarly, substituting Eqs. (24), (28), and (31) into the generalized law gives the low-aspect-ratio continuum-flow limit:

$$\Gamma = N^{-1/2}. \tag{33}$$

B. The plug-flow limit

For the other limiting case of scale, the flow becomes dominated by non-continuum and non-equilibrium effects, for liquids and dilute gases, respectively. For more information, see the reviews by Gad-el-Hak,[29] Karniadakis *et al.*,[34] and Conlisk.[35] The complexity of channel flow increases dramatically in such conditions, e.g., density layering can occur near to the bounding surface in nanoscale liquid channel flows[36] and Knudsen layers (kinetic boundary layers) can occur in rarefied-gas channel flows.[37] Furthermore, the state-of-the art simulation techniques for such flows—molecular dynamics for liquid and dense gas flows,[38] and the direct simulation Monte Carlo method for dilute gas flows[39]—although accurate, are extremely computationally expensive. Therefore, for the purpose of generating a simple analytical relation, we make use of the general approximate observation that at very small scales (i.e., small channel cross sections or high degrees of rarefaction), the channel velocity profile assumes a "plug-like" form, wherein the average velocity approximates the velocity of the fluid at the walls (the slip velocity). Navier's slip condition (which is only approximate for these conditions, as discussed in Section II C) allows us to express the wall shear stress τ_w as a function of the slip velocity u_s, which must be nearly constant around the perimeter of the cross section, given the plug-flow profile:

$$\tau_w = \frac{u_s \mu}{\eta}, \tag{34}$$

where η is the slip length determined by the fluid-solid interaction. Note the value of η does not affect the optimal area ratio solution at the plug-flow limit, and thus accurate knowledge of it is not required. As the flow tends to the plug-flow limit, the mass flow rate is simply

$$Q = \rho A u_s, \tag{35}$$

and a force balance relates the pressure drop to the wall shear, i.e.,

$$A\Delta P = L\tau_w \mathcal{P}, \tag{36}$$

where $\mathcal{P}$ is the perimeter of the section. Combining Eqs. (34)–(36) gives the mass flow rate

$$Q = \rho \eta A^{3/2}\left(\frac{\Delta P}{L}\right)\frac{R}{\mu}, \tag{37}$$

and the flow resistance per unit length

$$k = \frac{\mu}{\rho \eta R A^{3/2}}, \tag{38}$$

where $R = \sqrt{A}/\mathcal{P}$ is a property of the cross-sectional shape (like S).

1. Constant-shape networks

If we consider the case where the shape remains the same throughout the network, Eq. (38) can be substituted into the generalized law (16) to get the plug-flow limit for an arbitrary cross-sectional shape:

$$\Gamma = N^{-4/5}. \tag{39}$$

2. Constant-depth networks

For networks of rectangular cross section with a constant depth, Eq. (38) can be rewritten as

$$k = \frac{2\mu h(\alpha + 1)}{\rho \eta A^2}, \tag{40}$$

where the perimeter is

$$\mathcal{P} = 2h(\alpha + 1). \tag{41}$$

Noting again that $\alpha = A/h^2$, it can be seen from Eq. (40) that at the aspect-ratio limits, k reduces to

$$k = \frac{2\mu}{\rho\eta h A}, \text{ for } \alpha \gg 1; \tag{42}$$

$$k = \frac{2\mu h}{\rho\eta A^2}, \text{ for } \alpha \ll 1. \tag{43}$$

Substituting Eq. (42) into the generalized law gives

$$\Gamma = N^{-1} \tag{44}$$

for the high-aspect-ratio plug-flow limit. Interestingly, the high-aspect-ratio limits are the same for continuum- and plug-flow. Similarly, substituting Eq. (43) into the generalized law gives

$$\Gamma = N^{-2/3} \tag{45}$$

for the low-aspect-ratio plug-flow limit.

C. A slip flow approximation

In certain regimes, between the continuum- and plug-flow limits, it is sufficiently accurate to model the channel flow using Navier-Stokes equations with modified boundary conditions accounting for the velocity slip at wall boundaries—such solutions are referred to as *slip solutions*. There are number of types of slip boundary condition (see, e.g., those in Refs. 34 and 40), but the most common is Navier's slip condition (for which Maxwell's slip boundary condition[41] is a special case for gas flows). Slip solutions using Navier's condition ($\tau_w = u_s\mu/\eta$) have shown to yield accurate results, as compared to molecular dynamics predictions, for liquid flows in channels as small as ~1–2 nm for water[42] and ~2–3 nm for Lennard Jones fluids.[43,44] For gases, provided the Knudsen number (the ratio of the mean free path to the channel height) is small, the slip solution is also a well-known and good approximation.

A further approximation to the *exact* slip solution, for any cross section, can be obtained by assuming that the shear stress, and thus the velocity slip, is constant around the perimeter, i.e.,

$$Q \approx \frac{\rho\Delta P A^2}{L\mu\mathcal{P}}(S\mathcal{P} + \eta). \tag{46}$$

This gives the exact mass flow rate of the slip solution for a circular cross section (which has a uniform shear stress) and accurate approximations for rectangles of any aspect ratio (within 3% of results from a finite-difference slip solver). Note that the slip solution is itself an approximation, and particularly for gas flows must be treated with caution, as discussed later. Equation (46) can be rearranged to give the flow resistance per unit length

$$k = \frac{\mu\mathcal{P}}{\rho A^2(S\mathcal{P} + \eta)}. \tag{47}$$

Inserting Eq. (47) into the generalized law (Eq. (16)) for parent and daughter channels produces the general slip solution for the optimal daughter-parent area ratio for all cross-sectional shapes across all length-scales

$$\Gamma^3\left[\frac{\eta\left(2\mathcal{P}_p - A_p\frac{d\mathcal{P}}{dA}\Big|_p\right) + \mathcal{P}_p^2\left(A_p\frac{dS}{dA}\Big|_p + 2S_p\right)}{(S_p\mathcal{P}_p + \eta)^2}\right] = N^{-2}\left[\frac{\eta\left(2\mathcal{P}_d - A_d\frac{d\mathcal{P}}{dA}\Big|_d\right) + \mathcal{P}_d^2\left(A_d\frac{dS}{dA}\Big|_d + 2S_d\right)}{(S_d\mathcal{P}_d + \eta)^2}\right]. \tag{48}$$

1. Constant-shape networks

For all networks with a constant shape, $S_p = S_d$ and $dS/dA = 0$. For a circular cross section, $A = \pi R^2$, $S = 1/(8\pi)$, $\mathcal{P} = 2\sqrt{\pi A}$, and $d\mathcal{P}/dA = \sqrt{\pi/A}$. Substituting these values into Eq. (48) and simplifying produces

$$\Gamma^{5/2} = N^{-2}\left(\frac{\tilde{r}_p\sqrt{\Gamma} + 3}{\tilde{r}_p + 3}\right)\left(\frac{\tilde{r}_p + 4}{\tilde{r}_p\sqrt{\Gamma} + 4}\right)^2, \tag{49}$$

where $\tilde{r}_p = r_p/\eta$. For rectangular cross sections, $\mathcal{P} = 2(\alpha+1)h$ and $d\mathcal{P}/dA = (\alpha+1)h/A$. A constant shape means a variable depth h and a constant aspect ratio $\alpha = A/h^2$. Substituting these values into Eq. (48) and simplifying gives an optimal area relation of

$$\Gamma^{5/2} = N^{-2}\left(\frac{4C\tilde{h}_p\sqrt{\Gamma} + 3}{4C\tilde{h}_p + 3}\right)\left(\frac{C\tilde{h}_p + 1}{C\tilde{h}_p\sqrt{\Gamma} + 1}\right)^2, \tag{50}$$

where S is calculated using Eq. (26) $\tilde{h}_p = h_p/\eta$ and $C = 2S(\alpha + 1)$ is a constant.

2. Constant-depth networks

For rectangular cross sections of a constant depth and variable aspect ratio, substituting the expression for dS/dA (from Eq. (29)) into Eq. (48), along the rectangle parameters previously outlined, gives

$$\Gamma^3\left[\frac{2\tilde{h}(\alpha_p + 2) + 4\tilde{h}^2(\alpha_p + 1)\left(A_p\frac{dS}{dA}\Big|_p + 2S_p\right)}{\left(2\tilde{h}S_p(\alpha_p + 1) + 1\right)^2}\right] = N^{-2}\left[\frac{2\tilde{h}(\alpha_d + 2) + 4\tilde{h}^2(\alpha_d + 1)\left(A_d\frac{dS}{dA}\Big|_d + 2S_d\right)}{\left(2\tilde{h}S_d(\alpha_d + 1) + 1\right)^2}\right]. \tag{51}$$

III. NUMERICAL VERIFICATION AND DISCUSSION

An accurate numerical optimization procedure is now described to demonstrate the following: (a) the generalized law (Eq. (16)) is applicable to networks with arbitrary cross-sectional shape and for all scales; (b) the limits of the generalized law, identified as the continuum-flow limit (Eqs. (25), (32), and (33)) and the plug-flow limit (Eqs. (39), (44),

and (45)), are valid and precise for all shapes considered; and (c) the approximate slip solutions to the generalized law (Eqs. (49)–(51)) provide reasonable accuracy, even for rarefied gas flows.

The numerical optimization procedure is based on calculations that use non-dimensional mass flow rates, i.e.,

$$\tilde{Q} = \frac{Q\mu L}{\rho A^2 \Delta P}. \tag{52}$$

These mass flow rate are obtained either from published sources, from high-resolution finite-difference slip solutions, from exact analytical expressions, or from stochastic particle calculations (for dilute gases). The numerical model of the network also assumes that channels are sufficiently long such that pressure losses at the parent-daughters junction are negligible compared to the pressure drops over the channels themselves. This allows a model for a two-level network to be constructed from predictions of mass flow rate through individual channels, constrained by a common branching pressure and the requirement for mass continuity. For each shape and physical model, an interpolant is constructed that provides the non-dimensional mass flow rate for any given area, $\tilde{Q}(A)$. From this, Eq. (52) can be evaluated for parent and daughter channels

$$\Delta P_p = \frac{Q\mu L_p}{\tilde{Q}(A_p)\rho A_p^2}, \tag{53}$$

$$\Delta P_d = \frac{Q\mu L_d}{N\tilde{Q}(A_d)\rho A_d^2}. \tag{54}$$

Combining Eqs. (53) and (54), and substituting for the total pressure drop $\Delta P = \Delta P_p + \Delta P_d$, produces a model of the mass flow rate through a two-level network for a particular cross-sectional shape and physical model:

$$Q = \frac{\rho \Delta P}{\mu}\left[\frac{L_p}{\tilde{Q}(A_p){A_p}^2} + \frac{L_d}{N\tilde{Q}(A_d)A_d^2}\right]^{-1}. \tag{55}$$

For symmetric branching, the volume constraint requires that $L_p A_p = V - NA_d L_d$. The numerical procedure uses an interior-point constrained optimization algorithm[45] in MATLAB® to find the parent and daughter areas that, in combination, maximize the mass flow rate through the network (as predicted by Eq. (55)) for arbitrarily fixed total volume, total pressure drop, channel lengths, and fluid properties. Alternatively, the same result can be obtained via a brute force approach to ensure that the numerical optimization finds a global, not local, maximum.

A. Different shapes and sizes

Murray's original derivation was for circular channel sections at the continuum-flow limit. The first set of optimization results are presented to verify that the generalized law is valid for a variety of cross-sectional shapes across all length scales, with the shape remaining constant through branching. The numerical optimization uses non-dimensional mass flow rates calculated from a standard central-difference solution of the laminar Navier-Stokes equations with a Navier slip boundary condition.[46] The results from the analytical and numerical optimizations, for symmetric bifurcations, are presented in Fig. 2.

For large parent areas, relative to the square of the slip length η, the optimum daughter-parent area ratio converges to the continuum-flow limit of the generalized law (Eq. (25)) for all shapes considered. The same is true for the other extreme of scale: the optimum area ratio for all shapes converges to the plug-flow limit of the generalized law (Eq. (39)) for small parent areas. In the transition between these limits, the approximate slip solutions of the generalized law are also highly accurate. The difference between the slip approximations of the generalized law and the numerical optimization is less than 0.1% across the entire range of scales for all shapes tested. Clearly, predictions for the optimum dimensions are not particularly sensitive to errors introduced by the approximation in Eq. (46). These results are consistent regardless of the daughter and parent channel length magnitudes, demonstrating that the optimal daughter-parent area ratio is independent of the lengths, as was asserted in the analytical solution.

In Fig. 2, it is observed that for networks of channels with rectangular cross sections, the aspect ratio affects the range of areas for which Γ is in the transition period between the continuum- and plug-flow limits. This occurs because the influence of slip is governed by the size of the *smallest* cross-sectional length scale (hereon referred to as the characteristic length $\mathcal{L}$) relative to the slip length. So, for the same cross-sectional area, the characteristic length of a rectangle with a high-aspect-ratio is less than the characteristic length of a low-aspect-ratio rectangle. This means that optimal branching of high-aspect-ratio channels will depart from the continuum-flow limit and approach the plug-flow limit at larger parent areas than optimal branching in low-aspect-ratio channels.

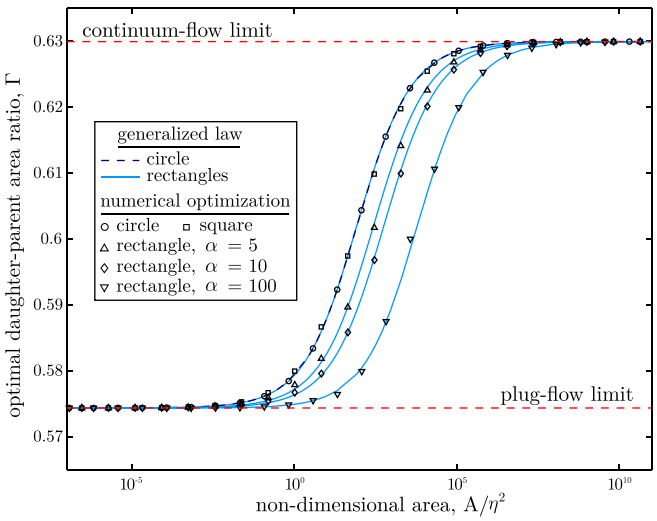

FIG. 2. Optimal daughter-parent area ratio Γ against non-dimensional parent area for networks with a constant shape. Comparison of the approximate slip solution to the generalized law (Eqs. (49) and (50)) and the numerical optimization using data from a Navier-Stokes slip solver. Plotted for circles, squares, and rectangles of aspect ratio $\alpha = 5$, $\alpha = 10$, and $\alpha = 100$ at $N = 2$.

B. Rarefied gas flow

The numerical optimization is now performed for symmetric branching of rarefied gas flows. The mass-flow-rate data are obtained from a variety of sources, including our own simulations[47] computed using a version of low-variance deviational simulation Monte Carlo (LVDSMC).[48] Additional mass-flow-rate data are procured from solutions of the linearized Boltzmann equation[49,50] to verify the accuracy of the LVDSMC results. For dilute gases, the slip length can be related to the mean free path λ via $\eta = C_s\lambda$, where $C_s = 1.11$ is the first-order slip coefficient for the hard-sphere model of gases with purely diffuse molecular reflection at walls.[51] The results for the analytical and numerical optimizations, for circular cross sections, are presented in Fig. 3. To demonstrate that the generalized law is valid for any number of daughter branches ($N \geq 2$), Γ is plotted for $N = 2$, $N = 3$ and $N = 5$ and, for clarity, is normalized with respect to the continuum-flow limit ($N^{-2/3}$).

Again, the agreement between the numerical optimization and the plug-flow limit of the generalized law is excellent for each case considered. It is perhaps unexpected that a slip solution to the generalized law should converge to the same result as that of kinetic theory and LVDSMC at the free-molecular limit, given the approximate nature of slip boundary condition at such scales. However, as $\tilde{r}_p \to 0$, Γ in Eq. (49) becomes independent of the slip length η, and is thus unaffected by any inaccuracy in the slip model. Due to computational cost, molecular simulations are not performed for sufficiently large areas to see the solution meet the continuum-flow limit; but, since the results from kinetic theory converge to the solution of the slip model, agreement at the continuum-flow limit is also expected. It is well known that when the Knudsen number $\mathrm{Kn} = \lambda/\mathcal{L}$ is greater than ~ 0.1, slip solutions become inaccurate, explaining the departure in Γ between the limits. The kinetic theory and LVDSMC results all show a minimum in Γ beneath the plug-flow/free-molecular limit. This is possibly a manifestation of the Knudsen minimum,[52] a rarefied gas phenomenon that occurs when the diffusive flux starts to dominate the convective flux as the length scale decreases.[53]

Note although Eq. (49) is approximate between the scale limits, the precise result of the numerical optimization can be reclaimed by expressing the interpolated dimensionless mass flow rate, $\tilde{Q}(A)$, as a flow resistance per unit length, $k(A)$. This allows the evaluation of the generalized law in (16), but, of course, does not afford an analytical relation.

C. Constant-depth rectangles

Finally, we perform a numerical optimization for a symmetrically bifurcating network of rectangular channels with a constant depth and variable aspect ratio, mimicking the conditions of a micro-fabricated fluidic network. Here, we have used non-dimensional mass-flow-rate data obtained from the two-dimensional Navier-Stokes slip solver. Figure 4 shows the optimum daughter-parent area ratio against dimensionless area (A/h^2; incidentally, this is equal to the aspect ratio, α) for rectangles of a constant dimensionless depth $\tilde{h} = h/\eta$.

Agreement between the numerical optimization and the approximate slip solution to the generalized law (Eq. (51)) is excellent for all cases, with the difference being less than 0.5% across the entire range of scales. The results also show convergence to the limits derived in Eqs. (32), (33), (44), and (45). It can be seen that when the non-dimensional depth $\tilde{h}$ is small, such that the slip length is relatively large, Γ varies only between the plug-flow limits for high and low aspect ratios (Eqs. (44) and (45), respectively). The high-aspect-ratio limits are the same for continuum- and plug-flow. When $\tilde{h}$ is large and the aspect ratio decreases, Γ first tends to the low-aspect-ratio limit continuum-flow (Eq. (33)), until the area gets sufficiently small that the variable width is comparable to the slip length, at which point

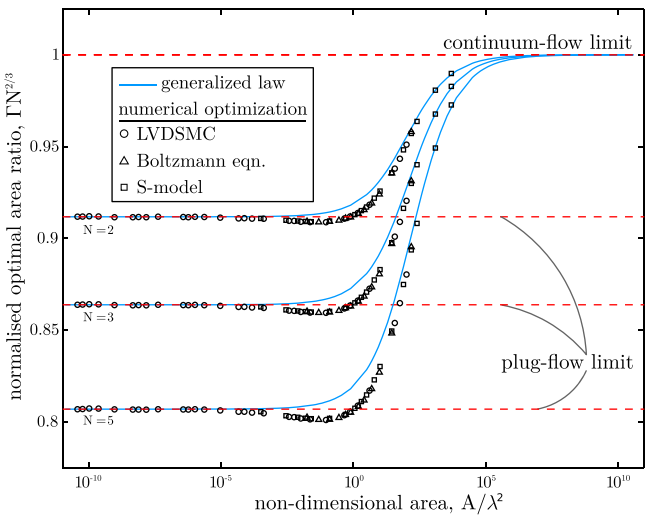

FIG. 3. Normalized optimal daughter-parent area ratio against non-dimensional parent area. Comparison of the analytical slip solution to the generalized law (Eq. (49)) and the numerical optimization using data from kinetic theory[49,50] and LVDSMC. Plotted for circles at $N = 2$, $N = 3$, and $N = 5$.

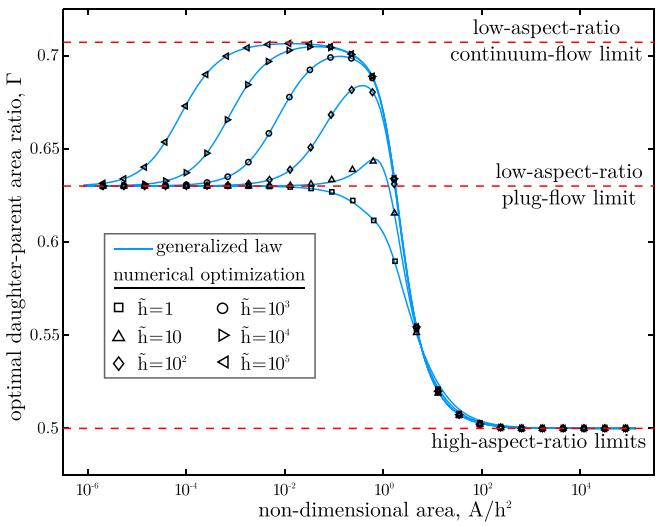

FIG. 4. Optimal daughter-parent area ratio Γ against non-dimensional parent area A/h^2 (equal to aspect ratio α) for rectangles of a constant dimensionless depth $\tilde{h}$. Comparison of the approximate slip solution to the generalized law (Eq. (51)) and the numerical optimization using data from a Navier-Stokes slip solver. Plotted for rectangles of depth $\tilde{h} = 1, 10, 10^2, 10^3, 10^4$, and 10^5, at $N = 2$.

the solution converges again to the low-aspect-ratio plug-flow limit (Eq. (45)).

For constant-depth networks, Γ behaves very differently compared to constant-aspect-ratio networks. For the most part, when the depth is constant, the optimal daughter-parent area ratio increases with decreasing cross-sectional area—the opposite to the trend found in Figs. 2 and 3. In addition, the range of Γ values is wider, the minimum Γ is smaller, and the maximum Γ is larger for constant-depth networks: $0.5 \leq \Gamma \leq 0.71$ compared to $0.57 \leq \Gamma \leq 0.63$. However, there are some similarities. At the low-aspect-ratio limits, the trend for constant-depth networks is the same as for constant-aspect-ratio networks, with the optimal daughter-parent area ratio decreasing as cross-sectional area decreases.

IV. CONCLUSION

We have derived a generalized optimization principle that leads to analytical expressions for the optimum daughter-parent area ratio Γ for any shape, at any scale, and for any number of daughter branches. We have shown that at the continuum-flow limit, Murray's law is reclaimed ($\Gamma = N^{-2/3}$) for networks of any cross-sectional shape, as long as the shape is constant through branching. The generalized law presented is also valid for slip flows and plug flows ($\Gamma = N^{-4/5}$) that occur at smaller length scales, as well as for networks with a constant depth, which is often a requirement for lab-on-a-chip devices due to limitations in fabrication procedures. The new optimal design relation we propose will allow the original biomimetic design principle of Murray to be applied to a variety of micro and nanofluidic networks that require non-circular geometry, due to manufacturing constraints, and are designed for increasingly smaller scales in order to achieve a greater degree of control, functionality, and analytical and economic efficiency. Future work will include determining optimal branching angles and optimum channel lengths for arbitrary cross-sectional shapes, across all physical scales.

ACKNOWLEDGMENTS

We would like to thank Professor David Emerson for useful discussions and Professor Nicolas Hadjiconstantinou for providing the original LVDSMC source code. This work is financially supported in the UK by EPSRC Programme Grant Nos. EP/I011927/1 and EP/K038664/1.

[1]C. D. Murray, Proc. Natl. Acad. Sci. U.S.A. **12**, 207 (1926).
[2]G. M. Hutchins, M. M. Miner, and J. K. Boitnott, Circ. Res. **38**, 572 (1976).
[3]G. S. Kassab and Y. B. Fung, Ann. Biomed. Eng. **23**, 13 (1995).
[4]M. LaBarbera, Science **249**, 992 (1990).
[5]T. F. Sherman, J. Gen. Physiol. **78**, 431 (1981).
[6]M. Zamir and N. Brown, Am. J. Anat. **163**, 295 (1982).
[7]M. Zamir and J. A. Medeiros, J. Gen. Physiol. **79**, 353 (1982).
[8]M. Zamir, J. A. Medeiros, and T. K. Cunningham, J. Gen. Physiol. **74**, 537 (1979).
[9]M. Zamir, S. M. Wrigley, and B. L. Langille, J. Gen. Physiol. **81**, 325 (1983).
[10]T. A. Wilson, Nature **213**, 668 (1967).
[11]K. Horsfield and G. Cumming, Bull. Math. Biophys. **29**, 245 (1967).
[12]K. Horsfield, F. G. Relea, and G. Gumming, Respir. Physiol. **26**, 351 (1976).
[13]K. A. McCulloh, J. S. Sperry, and F. R. Adler, Nature **421**, 939 (2003).
[14]K. A. McCulloh, J. S. Sperry, and F. R. Adler, Funct. Ecol. **18**, 931 (2004).
[15]K. A. McCulloh and J. S. Sperry, Am. J. Bot. **92**, 985 (2005).
[16]D. R. Emerson, K. Cieślicki, X. Gu, and R. W. Barber, Lab Chip **6**, 447 (2006).
[17]K. Tesch, Task Quarterly **14**, 227 (2010).
[18]L. Gosselin and A. K. da Silva, J. Appl. Phys. **101**, 114902 (2007).
[19]C. Renault, S. Colin, S. Orieux, P. Cognet, and T. Tzédakis, Microsyst. Technol. **18**, 209 (2012).
[20]A. Díaz Lantada, B. Pareja Sanchez, C. Gómez Murillo, and J. Urbieta Sotillo, Expert Rev. Med. Devices **10**, 629 (2013).
[21]S. M. Senn and D. Poulikakos, J. Power Sources **130**, 178 (2004).
[22]Y. Chen and P. Cheng, Int. J. Heat Mass Transfer **45**, 2643 (2002).
[23]X. Wang, A. S. Mujumdar, and C. Yap, Int. J. Therm. Sci. **45**, 1103 (2006).
[24]H. R. Williams, R. S. Trask, P. M. Weaver, and I. P. Bond, J. R. Soc. Interface **5**, 55 (2008).
[25]A. Kamiya and T. Togawa, Bull. Math. Biophys. **34**, 431 (1972).
[26]M. Zamir, J. Gen. Physiol. **69**, 449 (1977).
[27]A. Bejan, L. A. O. Rocha, and S. Lorente, Int. J. Therm. Sci. **39**, 949 (2000).
[28]D. Lim, Y. Kamotani, B. Cho, J. Mazumder, and S. Takayama, Lab Chip **3**, 318 (2003).
[29]M. Gad-el-Hak, J. Fluids Eng. **121**, 5 (1999).
[30]To find the optimal branching angle, a second optimization should be performed with the parent inlet and daughter outlets fixed, so the channel lengths and branching angle are functions of the branching point.
[31]In both of these cases, there is a non-linear relationship between the pressure gradient and the mass flow rate, however as at least one of these quantities must be constant in the optimization (see Eq. (8)), Eq. (16) is still valid.
[32]F. M. White, *Viscous Fluid Flow* (McGraw-Hill, 1974).
[33]C. Eloy, Phys. Rev. Lett. **107**, 258101 (2011).
[34]G. Karniadakis, A. Beskok, and N. Aluru, *Microflows and Nanoflows: Fundamentals and Simulation* (Springer, 2005).
[35]A. T. Conlisk, *Essentials of Micro- and Nanofluidics With Applications to the Biological and Chemical Sciences* (Cambridge University Press, 2012).
[36]C. Y. Soong, T. H. Yen, and P. Y. Tzeng, Phys. Rev. E **76**, 036303 (2007).
[37]D. A. Lockerby, J. M. Reese, and M. A. Gallis, Phys. Fluids **17**, 100609 (2005).
[38]M. P. Allen and D. J. Tildesley, *Computer Simulation of Liquids* (Clarendon Press, 1987).
[39]G. A. Bird, *Molecular Gas Dynamics and the Direct Simulation of Gas Flows*, Oxford Engineering Science Series Vol. 42 (Clarendon Press, 1994).
[40]D. A. Lockerby, J. M. Reese, D. R. Emerson, and R. W. Barber, Phys. Rev. E **70**, 017303 (2004).
[41]J. C. Maxwell, Philos. Trans. R. Soc. **170**, 231 (1879).
[42]L. Bocquet and E. Charlaix, Chem. Soc. Rev. **39**, 1073 (2010).
[43]K. P. Travis, B. D. Todd, and D. J. Evans, Phys. Rev. E **55**, 4288 (1997).
[44]C. Huang, P. Y. K. Choi, K. Nandakumar, and L. W. Kostiuk, J. Chem. Phys. **126**, 224702 (2007).
[45]R. A. Waltz, J. L. Morales, J. Nocedal, and D. Orban, Math. Program. **107**, 391 (2006).
[46]Our numerical solver is an in-house code written in MATLAB®, which uses matrix inversion to calculate the mass flow rates. All simulations use a 100×100 mesh, which has been shown (via a grid resolution study) to provide mass flow rate solutions to within 1% of the values obtained using a 200×200 and 300×300 mesh.
[47]For our LVDSMC simulations, periodic boundary conditions were used in the streamwise direction, 10 deviational particles were used per cell, and the cell size Δx was chosen to be $\lambda/5$. The time-step Δt was set to $\Delta x/\bar{c}$, where $\bar{c}$ is the most probable thermal velocity.
[48]G. A. Radtke, N. G. Hadjiconstantinou, and W. Wagner, Phys. Fluids **23**, 030606 (2011).
[49]S. K. Loyalka and S. A. Hamoodi, Phys. Fluids A **2**, 2061 (1990).
[50]F. Sharipov, J. Vac. Sci. Technol. A **14**, 2627 (1996).
[51]T. Ohwada, Y. Sone, and K. Aoki, Phys. Fluids **1**, 1588 (1989).
[52]M. Knudsen, Ann. Phys. **333**, 75 (1909).
[53]S. K. Mitra and S. Chakraborty, *Microfluidics and Nanofluidics Handbook* (CRC Press, 2012).